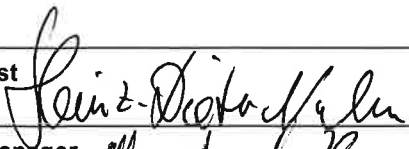


**Document Approval:****Date Approved**

Originator: Heinz-Dieter Nuhn, System Physicist		3/26/2014
Approver: Michael Rowen, Photon Systems Manager		3/31/14
Approver: David Schultz, Project Technical Director		3-31-14
Approver: Tor Raubenheimer, Physics Team Lead		3/31/14

Revision History

Revision	Date Released	Description of Change
R0	3/31/2014 <i>gw</i>	Original Release.

Table of Contents

1	Purpose	3
2	Scope	3
3	Definitions	3
4	References	3
5	Responsibilities	3
6	Overview	3
7	General Undulator Requirements	6
7.1	Segments.....	7
7.2	Break Section Components.....	12
7.2.1	Quadrupoles	13
7.2.2	Phase Shifters.....	14
7.2.3	Beam Position Monitors	14
7.2.4	Ambient Field Correctors.....	14
7.2.5	Beam Loss Monitors	15
7.3	Temperature and Position Stability.....	16
7.3.1	Temperature Monitoring	16
7.3.2	Gap Monitoring	16
7.3.3	Wire Position Monitors	16
7.4	Radiation Damage Issues	17
7.4.1	Damage Mechanisms	17



7.4.2	Radiation Protection.....	17
7.5	Vacuum System.....	17
7.6	Undulator Hall.....	19
7.7	Undulator Magnetic Tuning.....	19
7.8	Alignment.....	20
8	Alignment Strategy Overview.....	22
9	End Notes.....	23



1 Purpose

The *LCLS-II Undulator System Physics Requirements* document describes the requirements for the LCLS-II undulator system, which is the part of the LCLS-II beamlines that are located in the LCLS-II undulator hall.

2 Scope

The LCLS-II undulator system is comprised of two independent undulator beamlines, the hard x-ray undulator beamline (HXR) and the soft x-ray undulator beamline (SXR).

3 Definitions

BBA	Beam Based Alignment
FEL	Free Electron Laser
FODO	Focusing-Drift-Defocusing-Drift
SASE	Self-Amplified Spontaneous Emission
Undulator	Line of all Undulator Segments in a beamline (HXR or SXR)
Undulator Segment	The Individual undulator magnets (HXU or SXU)
HXU	Undulator Segment of the hard x-ray undulator beamline
SXU	Undulator Segment of the soft x-ray undulator beamline
Other terms defined in text	N/A

4 References

N/A	N/A
-----	-----

5 Responsibilities

N/A	N/A
-----	-----

6 Overview

The primary goal of LCLS-II is the production of two independent saturated SASE FEL photon beams, each with independently tunable photon energy. The photon energy will be controlled by both, the electron beam energy and the adjustable undulator gap. For a given electron energy, each undulator will be tunable over a large photon energy range independent of the other undulator. Each of the two undulators will receive electron beam bunches at an energy of about 4 GeV and at repetition rates of up to MHz from the same injector, superconducting linac, and transport lines alternatively directed into one of the two undulator beamlines just before reaching the undulator hall. In addition, the HXR beamline will alternatively receive electron beam bunches at energies in the 2.5 GeV – 15 GeV range at repetition rates of up to 120 Hz from the exiting Cu linac. The required tuning ranges are shown in Figure 1 and Figure 2.

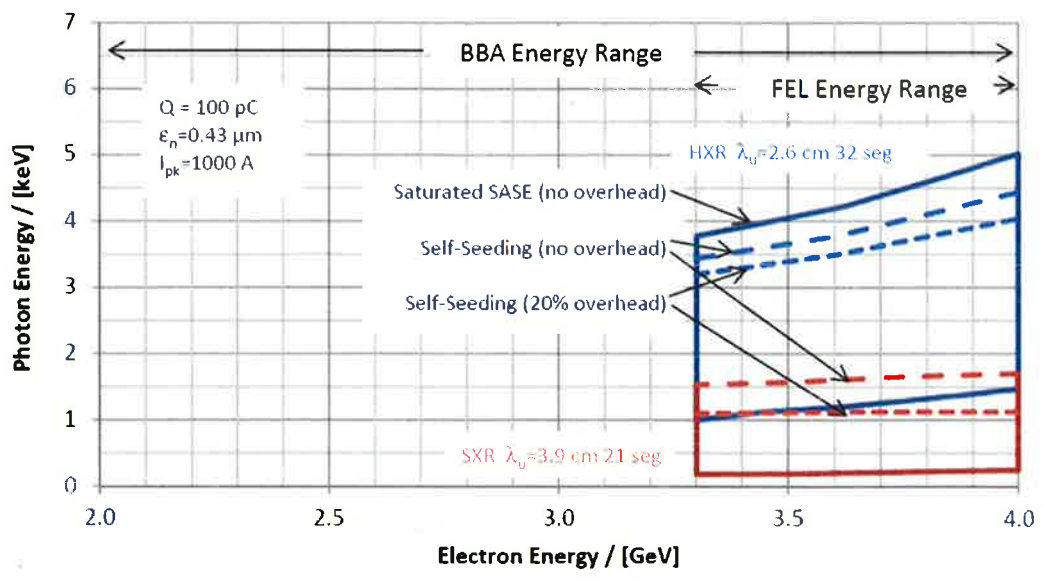


Figure 1: Ranges of available photon energy for the two LCLS-II undulator beamlines over the 3.3 GeV – 4.0 GeV electron energy range as provided by the superconducting linac system (SXR: red lines, HXR: blue lines). The lower range limits correspond to closed gap operation. The upper range limits are given by estimated saturation limitations, They can be pushed upwards by adding more undulator segments.

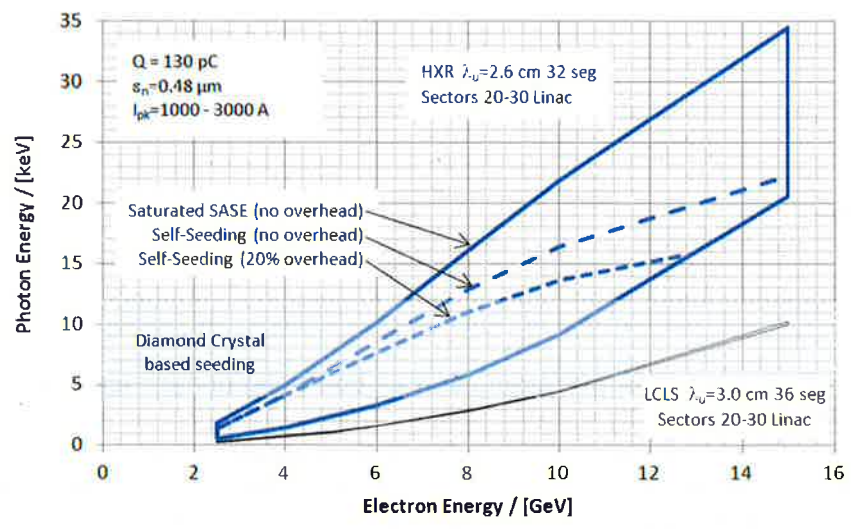
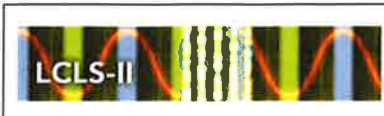


Figure 2: Photon energy ranges provided by the LCLS-II HXR undulator beamline over the 2.5 GeV – 15.0 GeV electron energy range as provided by the existing Cu linac system. The lower range limits correspond to closed gap operation. The upper range limits are given by estimated saturation limitations. They can be pushed upwards by adding more undulator segments. The black curves at the bottom indicates the range available with the existing LCLS 30mm period undulator.

Estimated divergence angles as function of photon energy are plotted in Figure 3 and Figure 4 based on FEL theory [1, Eq. (7)], using the photon energy, E_{ph} , the rms electron beam radius, $\sigma_{x,y}$, and the FEL power gain length, $L_{G,1D}$, with electron beam parameters as indicated in the figures.



$$\theta_{FWHM,x,\infty} = \frac{\sqrt{8 \ln(2)}}{\sqrt{\sigma_{x,y}^4 \sqrt{L_{G,1D}}}} \sqrt{\left(\frac{c \hbar}{2 E_{ph}}\right)^3} \quad (1)$$

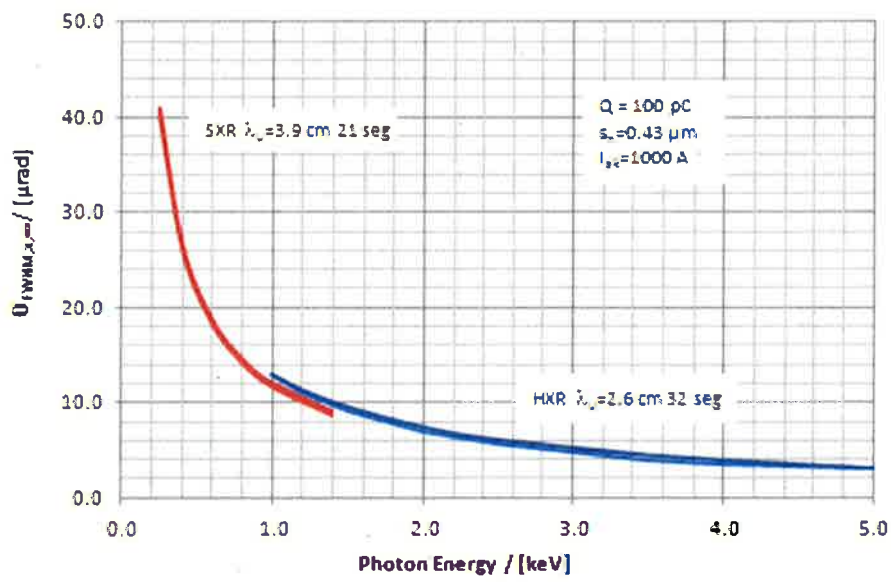


Figure 3: Nominal far-field divergence angles (full width at half maximum, FWHM) at saturation for the two undulators (red lines for SXR, blue lines for HXR) using the electron beam from the superconducting linac. Note: the indicated ranges are due to the corresponding electron energy ranges at the charge, emittance and peak current parameters specified in the figure. Working at different electron beam parameters can produce divergences outside the specified ranges.

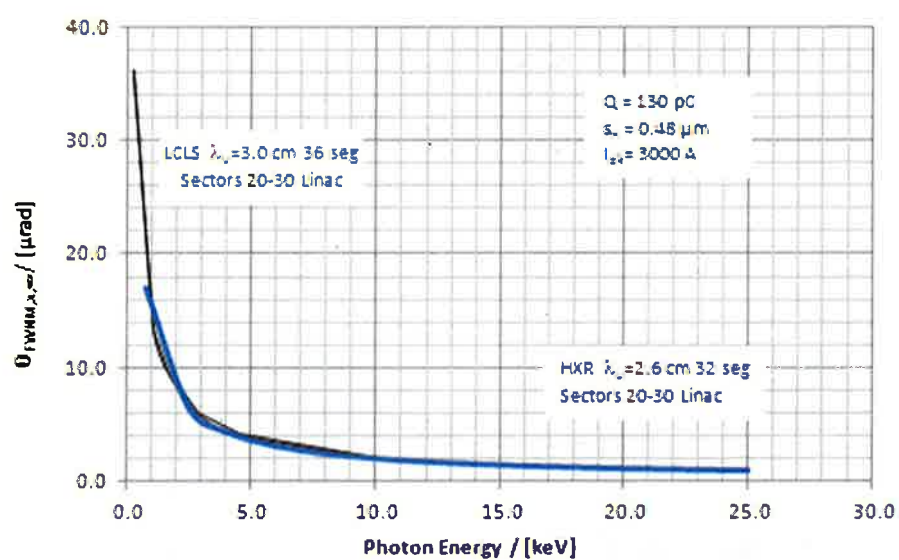


Figure 4: Nominal far-field divergence angles (FWHM) at saturation for the HXR undulator using the electron beam from the Cu linac. The values for the LCLS-I undulator are added in black for comparison.

For FEL operations to saturate, a set of demanding tolerances have to be met both by the undulator system itself and by the electron bunches delivered to the undulator system. The electron beam needs to be matched to the undulator FODO channels with the correct average beta-function as set by the undulator lattice and specified below. The main tolerances have been established and balanced in a tolerance budget, independently for each undulator beamline. This will be described in a separate document.

In addition to the FEL radiation, there will be a large amount of spontaneous radiation produced by the undulator systems over a broad spectral band. The intensity of the spontaneous radiation per bunch is only dependent on electron beam energy, E , electron bunch charge, Q , effective magnetic undulator field, B_u , and undulator length, L_u . The total spontaneous energy per bunch, integrated over all wavelengths and angles, can be calculated via

$$E_{spont} = 633 \frac{J}{GeV^2 T^2 m C} E^2 B_u^2 L_u Q \quad (2)$$

Table 1. Maximum spontaneous per pulse energy estimates for the proposed operational range.

Parameter	SXR/SCRF	HXR/SCRF	HXR/Cu	Unit
Min. Undulator gap	7.2	7.2	7.2	mm
Max. Electron beam energy	4.0	4.0	15.0	GeV
Max. Effective undulator magnetic field	1.51	1.01	1.01	T
Total effective magnetic undulator length	51.3	108.2	108.2	m
Nominal Electron bunch charge	100×10^{-12}	100×10^{-12}	250×10^{-12}	C
Total max. nom. spont. energy per pulse	0.000164	0.000111	0.00587	J

7 General Undulator Requirements

The LCLS-II undulator system is comprised of two independent undulators, the hard x-ray undulator (HXR) and the soft x-ray undulator (SXR).

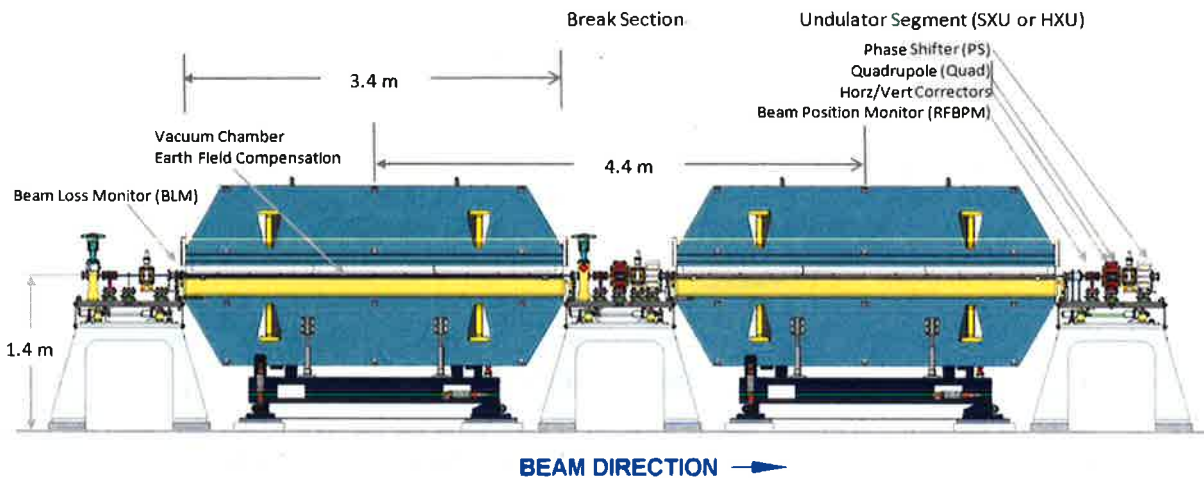


Figure 5: Schematic elevation view of segment and break section arrangements of each of the two LCLS-II undulators. The right handed coordinate system, used throughout this document, has the Z axis pointing in beam direction, the Y axis upwards and the X axis into the paper.



Each undulator (see Table 2) is comprised of individual undulator segments (HXU and SXU) separated by break sections (or interspaces), that will provide space for placing interspace components, i.e., a quadrupole (QU), an RF cavity beam position monitor (RFBPM), a phase shifter (PS), a collimator (COLL) and a beam loss monitor (BLM), as illustrated in Figure 5, plus various vacuum components. In addition, there will be one undulator quadrupole and two RFBPMs after the last segment, and also two RFBPMs upstream of the first undulators segments.

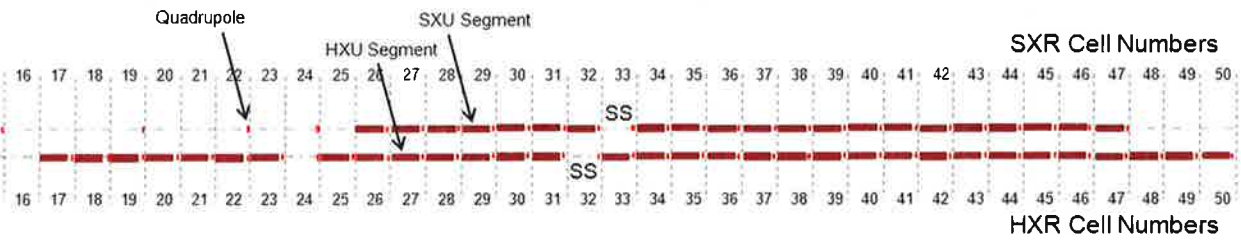


Figure 6: Schematic layout of segment and break section arrangements of each of the two LCLS-II undulators

Upstream of the SXR undulator proper, there will be a number of cells to allow future upgrade of the undulator line (see Figure 6). These cells will be sparsely populated with beam optics elements now, requiring only 4 additional break section-type quadrupoles. The segment numbers listed in Table 2 fulfill the minimum requirements for the estimated ranges listed in Figure 1 and are used throughout this document where applicable. The segment and interspace lengths have been used in tolerance calculations in this document. All undulator segments within each undulator beamline will use the same design.

Table 2. Basic undulator parameters

Parameter	SXR Values	HXR Values	Unit
Number of undulator segments	21	32	
Number of quadrupoles	22+4 ¹	34	
Number of RF cavity beam position monitors	22+3 ¹	34+3 ¹	
Number of Phase Shifters	20	31	
Number of beam loss monitors	21	32	
Break section length	1.00	1.00	m
Total magnetic undulator length	71.25	108.8	m
Total undulator length including interspaces	95.80	144.20	m

7.1 Segments

The undulator segments shall be planar variable strength permanent magnet type undulator magnets. The wiggle plane shall be oriented horizontally or vertically (the same for all segments). The basic parameters of the undulator segments are listed in Table 3.

¹ Added counts are components located before and/or after the regular undulator segment lattice.



Table 3. Basic undulator segment parameters

Parameter	SXU Values	HXU Values	Unit
Undulator period length (λ_u)	39	26	mm
Segment length	3.4	3.4	m
Number of effective periods per segment (N_p)	87	130	
Number of poles per segment	174	260	
Undulator type	Planar	Planar	
Undulator magnet type	PM Hybrid	PM Hybrid	
Gap type	Variable	Variable	
Magnet material	Nd ₂ Fe ₁₄ B	Nd ₂ Fe ₁₄ B	
Wiggle plane	horizontal	horizontal	
Magnetic Field Symmetry	antisymmetric	antisymmetric	
Minimum operational gap height	7.2	7.2	mm
On-axis vertical effective field at min. oper. gap	>1.51	>1.01	T
K_{eff} at minimum operational gap	>5.48	>2.44	
Minimum full open gap height	100	100	mm
Maximum operational gap height	22	20	mm
Minimum operational K values	1.24	0.44	

Table 4 lists tolerances for key quantities of each of the undulator segments: The “Vertical magnet array straightness” limits the systematic wander of the vertical pole positions along the undulators to avoid “banana-shape” and other deviations from a straight line. This tolerance insures that the space between the magnet poles and the vacuum chamber is not compromised. Alignment tolerances between individual segments as well as between the two strongback within a segment are listed separately, below, in Table 18 and Table 20.

Table 4. Undulator segment tolerance parameters (See caption of Figure 5 for coordinate definition.)

Parameter	SXU Values	HXU Values	Unit
Vertical (Y) magnet array straightness (rms)	<50	<50	μm
Longitudinal (Z) pole misalignment (rms)	<25	<25	μm
Total strongback deflection change (peak to peak)	<29	<19	μm

The “Longitudinal pole misalignment” tolerance refers to random longitudinal placement errors of each pole relative to its target position. The tolerance values have been taken from Figure 7, which shows that output power depends only weakly on pole placement errors. The tolerance values have been chosen because of achievability, larger tolerances can be negotiated, if required. The “Total peak to peak strongback deflection change” refers to parameter Δg_{defl} as discussed below. The tolerance values are from Figure 11.

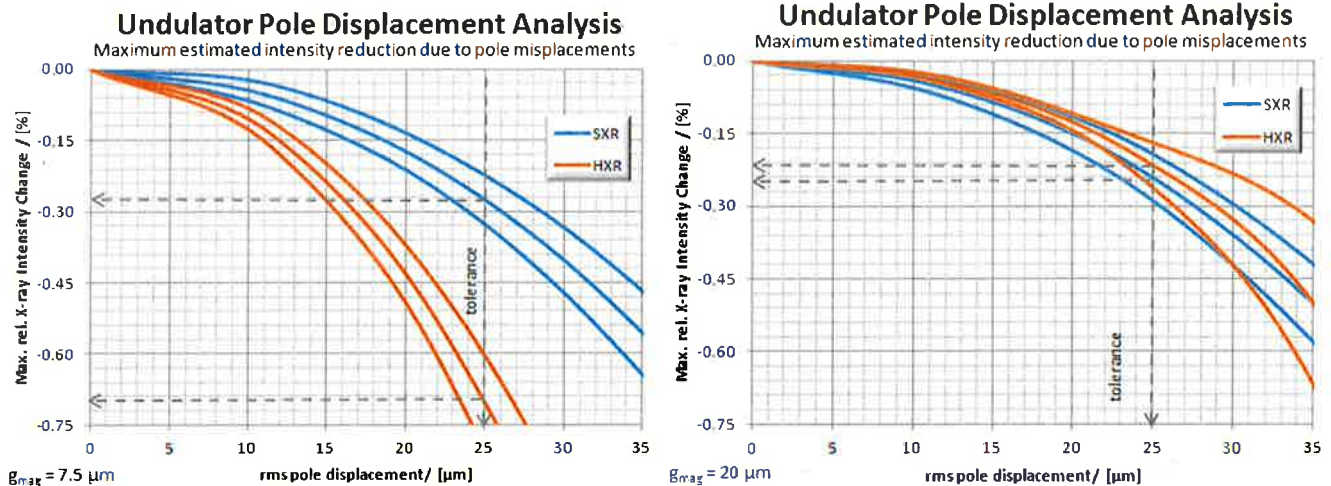


Figure 7: Change in x-ray intensity due to random longitudinal misplacements of individual undulator pole pieces. The plots are a result of computer simulations based on a single pole displacement signature as provided by D. Arbelaez, LBNL. The estimates are for two operational gap values (7.5 μm and 20 μm). An rms error of 25 μm keeps the performance reduction below the 0.75% level.

It is assumed each of the two undulator segment strongbacks will only be supported at discrete positions. The following analysis has been done for a two-point support as proposed by the LBNL group. The magnetic forces will cause deviations of the actual undulator gap from the requested gap due to z and gap dependent strongback deflections (see Figure 8) at z locations other than the support points. These deflections, in turn, will generate gap dependent changes to field integrals, total phase, phase shake, K_{eff} , and total power. The effect depends non-linearly on the gap, i.e., the strongest changes per gap change occur close to the minimum gap. Tuning will not be done at the minimum gap but at a slightly larger gap, which will be chosen such that the total phase error is roughly balanced, i.e., that absolute deviation in phase error at the smallest gap is roughly the same as the maximum at some intermediate gap.

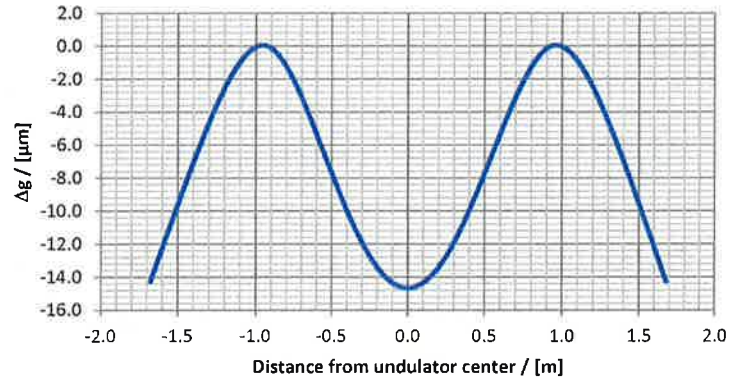


Figure 8: Change in undulator deflection with gap change. The vertical axis shows the maximum deviation of the actual full undulator gap from the requested gap when the requested gap is changed over the full range (i.e., between 7.2 mm and 200 mm).

The tuning procedure will cancel errors at the tuning gap. The strongback deflection tolerance is expressed as the maximum deviation from the nominal gap, Δg_{defl} , when changing that nominal gap between the minimum (7.2 mm) and the maximum gap (200 mm):

$$\Delta g_{defl} = \Delta g(g_{req}=200 \text{ mm}) - \Delta g(g_{req} = 7.2 \text{ mm}) \quad (3)$$

with

$$\Delta g(g_{req}) = \max(g_{act}(z, g_{req})) - \min(g_{act}(z, g_{req})). \quad (4)$$

g_{req} is the requested or nominal gap height and $g_{act}(z, g_{req})$ the actual gap height for a given requested gap, measured along z . The effects have been simulated and the results of the simulations for reduction in output power and change in phase error are shown in Figure 9 and Figure 10. In these figures, the stiffness of the strongbacks is characterized in the legends by the parameter Δg_{defl} . While changes in field integrals, total phase, and K_{eff} , can be measured and adjusted using correctors and gap control, the phase shake error, $\sigma_{\Delta\phi}$, which is the main source of total power reduction, can not be compensated. The reduction in total power can be used as a performance measure.

$$\sigma_{\Delta\phi} = \sqrt{\frac{1}{L} \int_0^L \Delta\phi(z')^2 dz'} = \frac{2\pi}{\lambda_u(1 + K_{eff}^2/2)} \left(\frac{e}{m_e c}\right)^2 \sqrt{\frac{1}{L} \int_0^L \Delta PI(z')^2 dz'} \quad (5)$$

The phase shake is defined as the rms of $\Delta\phi(z) = \phi(z) - \phi_0(z)$, the phase change, $\phi(z)$, along the actual undulator compared to the phase change, $\phi_0(z)$, along an error free ideal undulator. The phase, $\phi(z)$, of an electron relative to the radiation wave is defined as

$$\phi(z) = \frac{2\pi}{\lambda_r 2\gamma^2} \left(z + \left(\frac{e}{m_e c}\right)^2 PI(z) \right) = \frac{2\pi}{\lambda_u(1 + K_{eff}^2/2)} \left(z + \left(\frac{e}{m_e c}\right)^2 PI(z) \right), \quad (6)$$

i.e., in terms of the phase integral, $PI(z) = \int_0^z (I1_x(z')^2 + I1_y(z')^2) dz'$, which is calculated from the first field integrals

$$I1_{x,y}(z) = \int_0^z B_{x,y}(z') dz' - \frac{1}{L} \int_0^L B_{x,y}(z') dz'. \quad (7)$$

The second term on the right hand side in Eq. (7) is the average first field integral. Its subtraction emulates the action of BBA during operation. The intensity of the FEL power is related to the zero angle spectral intensity of the undulator radiation which is proportional to

$$|A|^2 = \left| \int_0^z I1_x(z') e^{-i\phi(z)} dz' \right|^2 + \left| \int_0^z I1_y(z') e^{-i\phi(z)} dz' \right|^2, \quad (8)$$

i.e., the product of the transverse velocity of the electron and the phase of the electromagnetic wave. It was found by Vinokurov et al. [ii] that a relative reduction of 4% in $|A|^2$ corresponds to a 1.1% reduction in FEL power gain length, which implies a 1.9% reduction of FEL output power. These results are compatible with simulation results published more recently by the European XFEL undulator group [iii]. The intensity change in the following figures is calculated via

$$\frac{\Delta P_{\text{sat}}}{P_{\text{sat}}} = 0.475 \times \frac{\Delta(|A|^2)}{|A|^2}, \tag{9}$$

Figure 9 and Figure 10 show estimated changes in intensity and total phase as a function of undulator gap relative to the tuning gap for the SXU and HXU segments. In these figures, it is assumed that the undulator magnets are perfectly tuned at the tuning gap, 10mm tuning gap for the SXR and 9mm for the HXR. As the gap heights are changed, jaw deflections cause the effects shown in the figures.

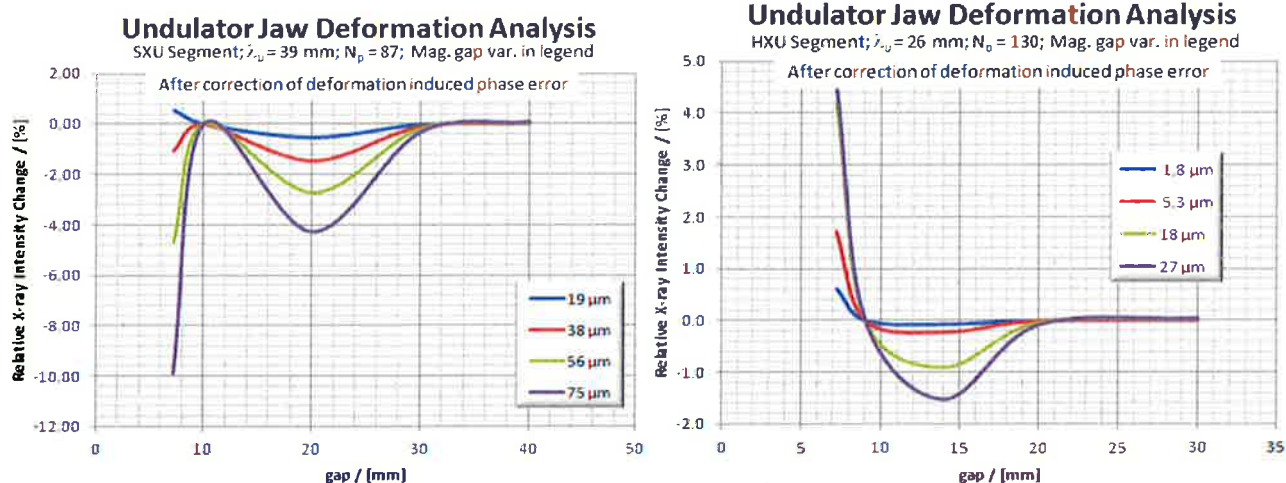


Figure 9: Relative change in the zero angle spectral intensity as function of gap for the SXU and HXU segments. The legend shows the change in peak-to-peak gap change due to strongback deflections when going from fully open to fully closed.

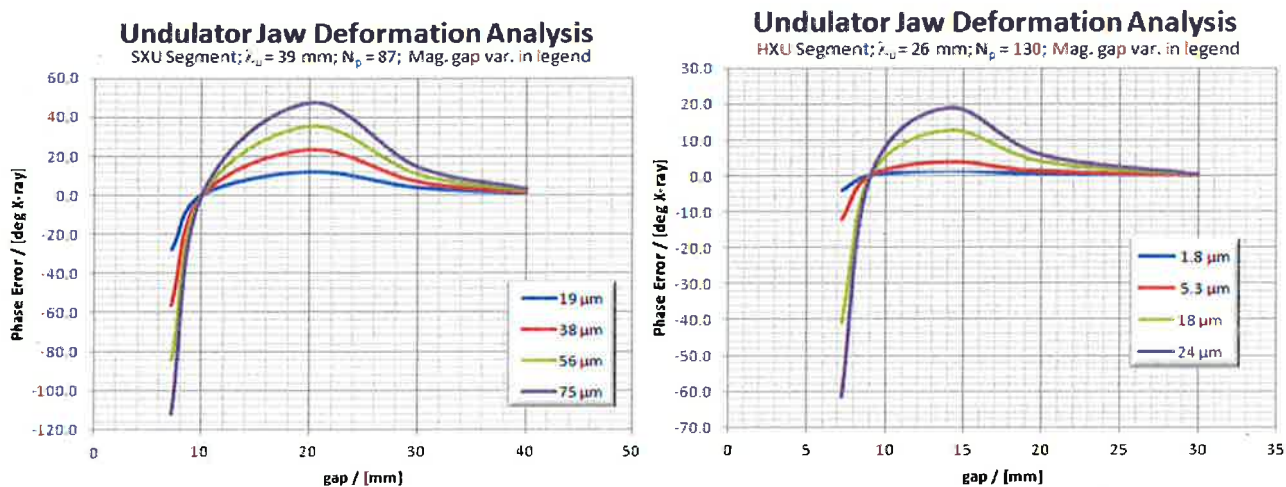


Figure 10: Change in phase error as function of gap for the SXU and HXU segments. The legend shows the change in peak-to-peak gap change due to strongback deflections when going from fully open to fully closed.

The figures illustrate the reason for choosing the tuning gap: the greatest impact of the deformation at gap heights of about 14 mm (HXU) and 21 mm (SXU) is reduced by allowing a similar reduction at the smallest gap of 7.2 mm. Tolerances at larger gap values are generally more stringent because larger gaps correspond to shorter radiation wavelengths. Figure 11 extracts tolerance information from Figure 9. The two curves in Figure 11 connect 4 data points



extracted from Figure 9 at the strongest deflection amplitudes for gaps larger than the tuning gap. The dashed lines mark strongback deflection for which a 1 % reduction in intensity occurs. If the actual deflections will be as large as those tolerances, the phase shifters will need to correct the corresponding gap dependent phase error, which is larger than the phase tolerance for those gap ranges.

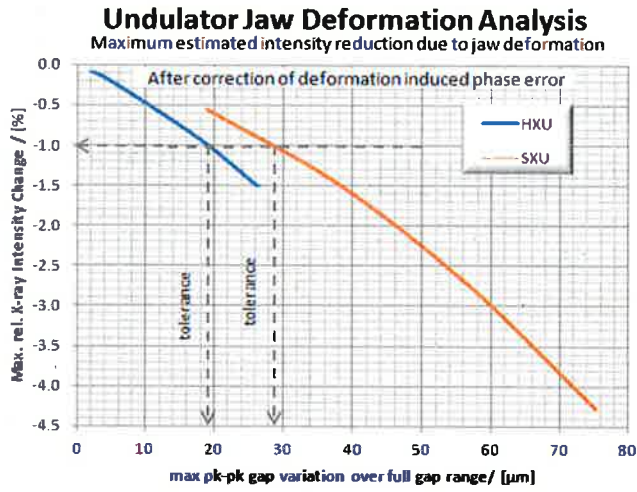


Figure 11: Change in x-ray intensity at the extremes of the curves in Figure 9 ($g=21$ mm SXU and $g=14$ mm HXU) as function of the maximum peak-to-peak gap variation as result of strongback deformation.

7.2 Break Section Components

In each break section, there will be components (i.e., quadrupoles, radio frequency cavity beam position monitors, phase shifters, radiation collimator, and beam loss monitors), that are necessary for controlling and monitoring the electron beam as well as monitoring radiation levels. Table 2 lists the total number for each component type.

These components will be mounted on a common support that can be precisely positioned by remote control (See page 22). Motion ranges and component stability during motion are listed in Table 5. As mentioned above, some of the interspace components are also required upstream and downstream of each undulator. Only those components between undulator segments and those directly preceding the first undulator segment and following the last undulator segments require motion control.

Table 5. Break section components mover parameters

Parameter	SXU Values	HXU Values	Unit
Horizontal motion range	± 1.0	± 1.0	mm
Horizontal motion accuracy (rms)	0.1	0.1	μm
Vertical motion range	± 1.0	± 1.0	mm
Vertical motion accuracy (rms)	0.1	0.1	μm
Horiz./Vert. vibration amplitude >1 Hz	<0.30	<0.25	μm
Roll stability over full motion range (rms)	<1	<1	mrad



7.2.1 Quadrupoles

The quadrupoles in both undulator lines will be air-cooled electro-magnets with laminated cores and three separate coil circuits: (1) Quadrupole (2) Horizontal Dipole Corrector (3) Vertical Dipole Corrector. The coils will be dimensioned such that heat dissipation to the tunnel air is minimized. The requirements for the quadrupoles are specified in Table 6. There, the item “Mag. center stability for $\Delta I_Q = \pm 20\%$ ” is needed when using the quadrupole excitation current to measure the amount of kick this quadrupole gives to the electron beam. That procedure scans of the quadrupole current amplitude by $\pm 20\%$ and measures the downstream electron beam trajectory to determine the kick amplitude. The item “Mag. center stability under corr. variation (rms)” implies that the actual magnetic center change produced by the corrector excitation current should not differ from the expected value by more than the specified amount.

Table 6. Quadrupole requirements

Parameter	SXU Values	HXU Values	Unit
Integrated gradient range	± 4.0	± 4.0	T
Quadrupole excitation current (I_Q) range	± 6.0	± 6.0	A
Mean gradient error	≤ 0.3	≤ 0.3	%
Gradient error (rms)	≤ 0.3	≤ 0.3	%
Magnetic center stability > 1 Hz	<0.25	<0.25	μm
Mag. center stability for $\Delta I_Q = \pm 20\%$	<1.0	<1.0	μm
Range of integrated horiz. corr. field (BI_{cux})	± 0.5	± 0.5	mTm
Range of integrated vert. corr. field (BI_{cuy})	± 0.5	± 0.5	mTm
Corrector excitation current range	± 1.0	± 1.0	A
Mag. center stability under corr. variation (rms)	<1.0	<1.0	μm
Maximum energy dissipation	<30	<30	W

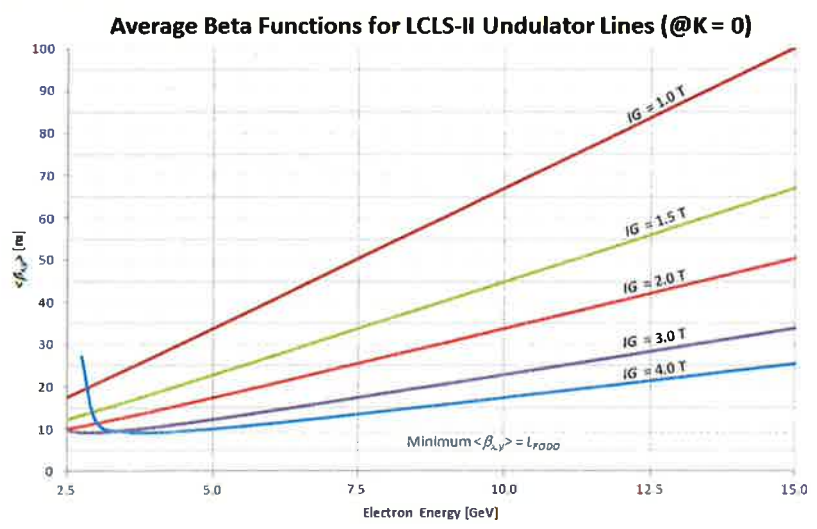
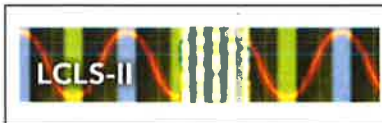


Figure 12: Average beta-functions over the operational energy range for the two undulators



Both LCLS-II undulator lines (HXR and SXR) use a FODO lattice to focus the electron beam and keep the average beta function constant along the undulator. Both FODO lattices have the same cell length of 4.4 m but can have different focal length. The average beta function required for optimum FEL gain is roughly proportional to electron energy for a given gap and undulator period. At a constant (but small) strength of focusing quadrupole magnets, the beta function will be proportional to electron beam energy. Also, the beam-based-alignment algorithm favors a constant quadrupole gradient. Therefore, at LCLS-II, as was the case at LCLS-I, the FODO lattice will operate a constant gradient. The integrated quadrupole gradients (IG) can be independently chosen for each undulator line but will be kept invariant with energy changes in support of BBA. The integrated quadrupole gradient needs to be below about 2.5 T for superconducting linac operation, while for Cu linac operation higher gradients can be used at a loss of the very low energy range. Figure 12 demonstrates how average beta function depends on beam energy and quadrupole gradient.

7.2.2 Phase Shifters

As the electrons travel through an undulator segment, their phase in the pondermotive well of the x-ray radiation field slips by exactly one x-ray wavelength for every undulator period travelled. As the gap of the undulator or the electron beam energy is changed, the radiation wavelength will adjust itself to maintain this condition. As the electron and x-ray beams transverse the field-free space in the interspace sections the electrons' phase change will be a function of the gap of the previous undulator and, therefore, be mismatched for most gaps. This needs to be corrected by phase shifter devices, installed in each break section between undulator segments. Requirements for the phase shifters are specified in a separate PRD [iv] to be released.

7.2.3 Beam Position Monitors

The capability to precisely measure the transverse position of each individual electron bunch to sub-micron precision is essential for the application of electron beam base alignment (BBA). The Radiofrequency Cavity Beam Position Monitors (RFBPMs) used for LCLS provide sufficient resolution of better than 250 nm. The use of a similar design is encouraged. Alignment can take advantage of the fact that the RFBPM body has circular shape and that the mechanical center of the device coincides with the center of the circular body shape that can be observed when the device is installed. It is important that an RFBPM is installed next to every undulator quadrupole. Two RFBPMs also need to be installed before the first and after the last undulator segment, as well as one RFBPM in each dump line.

7.2.4 Ambient Field Correctors

There will be small magnetic fields present in the undulator hall other than those intentionally created by the beam steering magnets than can modify the electron beam trajectory. The dominant sources are the earth magnetic field and magnetic components such as vacuum pumps, motors and magnetized steel pieces. The amount of trajectory errors that these fields will generate will depend on the locations of those magnetic components and on the gap height of the undulator segment. In the case of the earth field, those extra field components will be distributed more or less homogenously along the vacuum chamber and will deflect the electron beam onto a circular trajectory.



Table 7. Ambient Field Corrector Parameters

Parameter	SXU Values	HXU Values	Unit
Maximum B_x corrector field	± 0.6	± 0.6	G
Maximum B_y corrector field	± 1.4	± 1.4	G
Horizontal corrector wire center separation	14.2	14.2	mm
Vertical corrector wire center separation	5.0	5.0	mm
Maximum current for B_x corrector field	± 1.0	± 1.0	A
Maximum current for B_y corrector field	± 1.4	± 1.4	A
Maximum wire current	± 2.4	± 2.4	A
Maximum dissipated power per undulator segment	1.3	1.3	W
Estimated vacuum chamber temperature rise	0.2	0.2	K

The BBA procedure (see below) will mitigate the effect, by reducing the trajectory deviations at the positions of the BPMs, thereby creating a scalloped trajectory through the undulator segments. Those scalloped trajectories still cause a position dependent increase in path length and thus introduce a phase shake along the segment and a phase error with respect to the following segment. They also affect the convergence of the BBA procedure. In order to mitigate this effect, dipole steering coils will be integrated in the segment vacuum chamber as described in an LCLS Technical Note [v]. If powered with 2 independent power supplies, 4 copper wires mounted at the corners of the segment beam pipe can provide independently controllable horizontal and vertical corrector fields that are roughly constant along the beam axis. Based on XFEL measurements that used large Helmholtz coil arrangements to emulate the external fields, corrector field requirement increases with gap, maximum values of $B_x = 0.6$ G and $B_y = 1.4$ G should be sufficient for all cases. Relevant parameters for the vacuum chamber correctors are listed in Table 7.

The dependence of the corrector strength on undulator segment gap height can be determined during operations based on the reading of downstream RFBPMs. This method will only provide information for relative corrector strength change requirements, though, but will not provide information for the required absolute corrector strength. Those absolute corrector strength values can only be obtained based on measurements of the magnetic fields along the beam axis when the undulator segments are installed in the tunnel and set to a known gap before the vacuum chamber is installed. The required corrector setting at that gap can be calculated based on the difference of those measured fields to the equivalent fields measured in the magnet measurement facility with the same gap during tuning.

7.2.5 Beam Loss Monitors

Protecting the magnetic material from demagnetization due to radiation generated by the electron beam is very important for a continuous and reliable operation of the facility. Beam Loss Monitors (BLMs) that are integrated in the facility's Machine Protection System (MPS) are instrumental in protecting the undulators. The MPS is to be configured to prevent the electron beam from entering the undulator hall if radiation levels, as detected by the BLMs, exceed a threshold. The devices can be constructed very similarly to those used to protect the LCLS-I undulator, i.e., a quartz Čerenkov radiator, monitored with a photomultiplier. The shape of the radiator needs to be improved to reduce the sensitivity gradient that the existing BLM exhibit [vi].

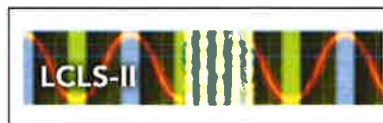


Table 8. BLM requirements

Parameter	SXU Values	HXU Values	Unit
Photon energy detection threshold	>1	>1	MeV
Lowest detectable deposited dose per pulse	1	1	pGy
Shielding factor for photons below 1 MeV	>1000	>1000	

The data acquisition system must be set up for continuous integration of the BLM signals. An upstream wire monitor can be used to calibrate the trip points of the beam loss monitors.

7.3 Temperature and Position Stability

7.3.1 Temperature Monitoring

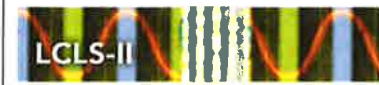
It is important that the local undulator temperature stays stable to within a ± 0.1 K. A temperature gradient is acceptable as long as the temperature at any given point is stable. The temperature of each undulator segment needs to be monitored redundantly. Each of the two strongbacks (magnet arrays) of each undulator segment needs to be equipped with three independent temperature sensors, each with an accuracy of 0.1 K after calibration. The total long-term drift shall stay within a ± 0.05 K range. In addition, each of the two jaws (magnet arrays) of each phase shifter needs to be equipped with a sensor of the same resolution and long-term drift stability as the undulator segment temperature sensors. Additional temperature sensors are needed to monitor each of the vertical support pillars for the undulator, the break section support, phase shifter, quadrupole, and the ambient air at each undulator segment.

7.3.2 Gap Monitoring

The gap height settings of the undulator segments and the phase shifters need to be monitored with absolute linear encoders with a repeatability of better than 1- μ m, while for the phase shifter, a single encoder for gap height will be sufficient. The undulator segments require gap height and mid-plane position encoders on both ends of each device.

7.3.3 Wire Position Monitors

X-ray FELs demand that the positions of undulator components be stable to less than 1 μ m per day. A precise wire position monitor system (WPM) has been developed and incorporated into the LCLS-I undulator line. This system is capable of measuring x, y, roll, pitch and yaw of each of the 33 undulator quadrupoles with respect to 140-meter-long stretched wires. Instrument resolution is about 10 nm and instrument drift is negligible [vii]. Position data of individual quadrupoles can be correlated along the entire 132-meter-long undulator. Even though the measurements showed that the underground tunnel is sufficiently stable to not require a closed loop feedback system based on the wire position monitor readings, the WPM allows monitoring and correcting this important tolerance of the FEL system. The LCLS-I WPM helped identify and characterize the source of quadrupole motion (e.g., coupling to Linac to Undulator, LTU ground motion, girder twist from segment roll in/out activity). Provisions are to be made for the future installation of an adapted version of the existing system for the LCLS-II HXR beamline, and a second system will be installed on the LCLS-II SXR beamline.



7.4 Radiation Damage Issues

7.4.1 Damage Mechanisms

In LCLS-I, undulator segments are being removed from the beamline and remeasured at the MMF on an on-going bases. These measurements show a reduction in $\Delta K/K$ at a rate of about 0.01% over 4 years. At the same time, radiation levels are integrated along the undulator line showing a steady dose rate during the beam operation rate of 120 Hz. with up to 250 pC bunch charge. Due to its high repetition rate planned for LCLS-II, there will be up to 1000 times more electrons per second in the LCLS-II beam than there are in the LCLS-I beam.

7.4.2 Radiation Protection

To protect the undulator magnet material from damage several protective measures will be implemented, similar to what is used in LCLS. They consist of:

- A complete collimator system upstream of the final bends in the LTU to limit the five-dimensional phase space (x, x', y, y', E), such that electrons that pass the collimator system will not be able to get lost in the undulator vacuum pipe if the undulator system components are set correctly.
- A machine protection system (MPS) based on the BLMs and RFBPMs to prohibit beam operation at high radiation doses or with trajectory amplitudes outside a ± 1 mm envelope.
- A collimator in front of each undulator segment.

7.5 Vacuum System

The LCLS-II undulator vacuum system needs to be operated at a pressure better than 10^{-6} Torr in order to keep bremsstrahlung and emittance growth to a minimum. To achieve this, an ion pump needs to be installed in each interspace section. The pump speed inside the narrow segment chamber is expected to be limited by the conductance.

Table 9. Undulator segment chamber vacuum parameters

Parameter	Values	Unit
Maximum vacuum pressure	1×10^{-6}	Torr
Segment chamber material	Aluminum ²	
Segment chamber inner cross section	Race-track	
Segment chamber inner height	5	mm
Segment chamber inner width	11	mm
Beam stay clear radius	2.3	mm
Segment chamber straightness	± 100	μm
Segment rms longitudinal surface roughness slope, α_z	<15	mrad
Segment rms azimuthal surface roughness slope, α_θ	<30	mrad
Number of horizontal chamber corrector coils (CUXs)	1	
Number of vertical chamber corrector coils (CUXs)	1	
Maximum resistive wall wakefield heating at 120kW beam	0.82	W/m

² Because of AC component of the resistive wall wakefield, Al is slightly better than Cu but much better than Au.

The mechanical vacuum chamber requirements are dominated by wakefield considerations. The interaction between the electron beam and the vacuum chamber generates longitudinal and transverse wakefields (characterized through the vacuum chamber impedance) that can reduce FEL gain and need to be kept small. There are three main contributors to the vacuum chamber impedance:

- electrical surface conductivity
- surface roughness
- geometric shape

The goal is to keep the contribution from surface roughness and geometric shapes small compared to the unavoidable contribution from the resistive wall conductivity. One component of the latter, ac conductivity [viii], can be reduced by the choice of aluminum as surface material. The same requirements apply for the vacuum system of both, the SXU and HXU vacuum system.

The surface roughness slope needs to be monitored by surface scans performed on small chamber samples during the vacuum chamber fabrication process. These scans will yield the surface height $h(z_i, \theta_j)$, which can be used to derive the rms surface roughness slopes (shown for the longitudinal):

$$\alpha_z = \sqrt{\frac{1}{n(n-1)} \sum_{j=1}^m \sum_{i=1}^{n-1} \left(\frac{h(z_{i+1}, \theta_j) - h(z_i, \theta_j)}{z_{i+1} - z_i} \right)^2} \quad (10)$$

Table 10. Undulator quadrupole chamber vacuum parameters

Parameter	Values	Unit
Maximum vacuum pressure	1×10^{-6}	Torr
Quadrupole chamber inner surface material	Aluminum	
Quadrupole chamber Al plating thickness	>100	nm
Quadrupole chamber inner cross section	Circular	
Quadrupole chamber inner diameter	>8	mm
Quadrupole rms longitudinal surface roughness slope	<60	mrاد
Quadrupole rms radial surface roughness slope	<100	mrاد
Quad chamber transv. pos error (rms)	<70	μm

Table 11. Undulator RFBPM vacuum parameters

Parameter	Values	Unit
Maximum vacuum pressure	1×10^{-6}	Torr
RFBPM inner surface material	Copper	
RFBPM total length estimate	~100	mm
RFBPM chamber inner cross section	Circular	
RFBPM chamber inner diameter	>8	mm



RFBPM rms longitudinal surface roughness slope	<60	mrاد
RFBPM rms radial surface roughness slope	<100	mrاد
RFBPM transv. pos error (rms)	<50	μm
RFBPM roll error (rms)	<1	mrاد

Table 12. Requirements for other undulator vacuum system components

Parameter	Values	Unit
Maximum vacuum pressure	1×10^{-6}	Torr
Other components chamber inner diameter	>11	mm
Other components chamber inner surface thickness	>100	nm
Other components inner surface material	Arbitrary	
Other components chamber inner cross section	Arbitrary	
Other components rms longitudinal surface roughness slope	Arbitrary	
Other components rms radial surface roughness slope	Arbitrary	

7.6 Undulator Hall

The undulator hall temperature and floor stability are a concern. It is important that the local undulator temperature stays reasonably stable. A temperature gradient is acceptable as long as the temperature at any given point is stable. Floor stability is very important since component position monitoring will not be available. Random movement of quadrupoles by 8 μm (rms) will *reduce FEL output by about 40%*, requiring another application of BBA. The table summarizes the requirements.

Table 13. Basic undulator hall requirements

Parameter	Values	Unit
Local temperature stability ΔT	± 0.1	°C
Maximum temperature variation along undulator line	± 1.0	°C
Average undulator temperature	20	°C
Differential floor stability between points separated by 10 m	± 0.2	μm/day

7.7 Undulator Magnetic Tuning

In order for the SASE process to produce optimum gain, four tuning considerations need to be satisfied for each operational gap:

1. Control of the undulator parameter, K_{eff} .
2. Phase shake reduction throughout each segment.
3. Reduction of the overall phase error across each segment.
4. Reduction of the first and second integrals of the horizontal and vertical field components.



Table 14. Basic undulator segment tuning requirements

Parameter	SXU Values	HXU Values	Unit
Undulator parameter tolerance $\Delta K_{eff}/K_{eff}$	$\pm 3.0 \times 10^{-4}$	$\pm 1.5 \times 10^{-4}$	
Horizontal K sextupole $ \frac{1}{2}(1/K_{eff}) \partial^2 K_{eff} / \partial x^2 $	$< 6.8 \times 10^{-4}$	$< 3.4 \times 10^{-4}$	1/mm ²
Tuning Gap height	10	9	mm
Tuning good field radius	1	1	mm
Cell length (L_{cell}) at tuning gap height	5.940^3	3.5483	m
Phase shake (rms) over L_{cell}	± 5.0	± 4.0	deg Xray
Cell phase error	± 10.0	± 5.0	deg Xray
First field integral of B_y per cell (abs)	< 40	< 40	μTm
Second field integral of B_y per cell (abs)	< 50	< 50	μTm^2
First field integral of B_x per cell (abs)	< 40	< 40	μTm
Second field integral of B_x per cell (abs)	< 50	< 50	μTm^2
Field integral quadrupole (abs)	< 0.01	< 0.01	T
Field integral sextupole (abs)	< 2	< 2	T/m
Field integral octupole (abs)	< 400	< 400	T/m ²

The phase errors are based on the segment cell length, L_{cell} , which is defined as the length of a line along the magnetic segment axis over which the total phase slippage is πN_p for the Tuning Gap height, when centered longitudinally at the segment center. N_p is the number of segment poles per strongback. A consequence of the field integral tolerances in

Table 14 is that differences between environmental field components (earth field etc.) in the undulator hall and those in the magnet measurement facility need to be smaller than 0.1 G, which is very likely not going to be the case without special effort (see section about beam pipe correctors, above). The Undulator parameter, and the phase shake are determined over the segment core, i.e., without considering the end sections.

7.8 Alignment

In order for the SASE process to produce optimum gain, three main alignment considerations need to be satisfied:

1. Align the quadrupoles such that the electron trajectory is straight, in order to reduce phase errors and improve overlap between the electron and photon beams.
2. Center the vacuum chamber to the electron beam to minimize emittance degradation from transverse wakefields.
3. Center the undulator to the beam to minimize errors in of the undulator parameters (K_{eff}).

All alignment operations will be based on the magnetic or electrical centers (rather than the mechanical shape, with the exception of RFPMs) of the components, which will be determined

³ The exact value will be determined during Prototype tuning.



in a separate process and fiducialized to tooling ball (sockets) or appropriate features on the device body.

The tolerances are listed in Table 15. Transverse quadrupole alignment is specified with respect to a virtual straight line. The local straightness requirements refer to a z interval of 10 m (roughly one HXR field gain length), while global straightness requirements refer to the total undulator length. It is assumed that initial alignment, based on conventional metrological methods, will provide good local straightness but might suffer from some degree of random walk-off, globally. The quadrupoles are the main focus of the alignment procedure; the other components will be aligned with respect to the quadrupoles. The final alignment tolerances for the quadrupoles are extremely tight and will be met by using electron beam based alignment in a similar way as with LCLS. A brief summary of the LCLS-II alignment concept is given in the next section.

Table 15. Basic quadrupole alignment requirements with respect to the reference coordinate system

Parameter	SXU Values	HXU Values	Unit
Initial quadrupole alignment (x,y)	±175	±175	µm
Final quadrupole position settability (x,y)	±1.5	±1.0	µm
Quadrupole x/y position stability (rms)	±15	±1.0	µm
Roll tolerance (rms)	<1.0	<1.0	mrad
Pitch tolerance (rms)	<15	<15	mrad
Yaw tolerance (rms)	<15	<15	mrad

Table 16. Undulator alignment requirements relative to electron beam trajectory

Parameter	SXU Values	HXU Values	Unit
Vert. mag. segment axis alignment	±200	±87	µm
Horiz. mag. segment axis alignment	±572	±300	µm
Segment roll tolerance (rms)	<1	<1	mrad
Segment pitch tolerance	±170	±50	µrad
Segment yaw tolerance	±500	±260	mrad
Segment chamber vert. mid-plane (rms) ⁴	<50	<60	µm

Table 17. Alignment and stability tolerances of upper jaw with respect to lower jaw

Parameter	SXU Values	HXU Values	Unit
Yaw error	±10	±1.75	mrad
Pitch error	±50	±17	µrad
Roll error (rms)	<4	<1	mrad
Horizontal position error (rms)	<400	<400	µm
Gap height error (rms)	<5	<1.5	µm

Table 18. Miscellaneous alignment tolerances

Parameter	SXU Values	HXU Values	Unit
-----------	------------	------------	------

⁴ Assuming segment chamber straightness tolerance of ±140 µm (rms)



Undulator z position tolerance (rms)	1.0	0.3	mm
--------------------------------------	-----	-----	----

8 Alignment Strategy Overview

The LCLS alignment strategy [ix] has been very successful in producing a straight electron beam trajectory sufficient for high FEL gain using a BBA procedure based on variable electron energies. LCLS-II will use a quite similar strategy even though there are system differences, such as variable gap and large undulator size, which require special considerations. The alignment concept for both, the SXR and the HXR segments will be similar. The core feature of the alignment concept is the same electron beam based alignment as is done for LCLS, which measures the trajectory for 4 different electron energies. For the LCLS-II HXR line, these electron energies will span the range between 4.2 GeV and 13.5 GeV. For the LCLS-II SXR line those energies will need to be chosen from the narrow range of 2 – 4 GeV. None of the undulator fields (i.e., quadrupole gradients, corrector strength, undulator gaps) will be varied during the measurements. For a given setting of the accelerator energy, the trajectory will be measured. As a result of these 4 sets of trajectory measurements, the BPM offset errors and quadrupole position errors are calculated and independently corrected for each line. The correction of the BPM offsets will be done by changing the values of process variables in the control system.

The quadrupole position errors will be corrected by remotely adjusting the quadrupoles' positions. In order to make these adjustments possible, each quadrupole, together with all the other break section components, i.e., BPM, phase shifter etc. will be mounted on a common support structure which can be remotely positioned with cam movers, similar to how the LCLS girder positions are controlled. This procedure will align the quadrupoles with sufficient precision such that the electron beam path gets straightened. This is expected to cause the electron beam to pass the quadrupoles very close to their magnetic axes. A small offset on the order of 20 μm (rms) will remain, just enough so that the small fields related to those offsets compensate any additional remnant field integrals that exist outside of the quadrupoles, i.e., coming from the remnant field integrals of the undulators and phase shifters, from the earth magnetic field, and from any other environmental field components. The tolerances for the fields outside the quadrupoles are 40 μTm for the first and 50 μTm^2 for the second field integrals. The field integrals from the earth magnetic field will exceed these tolerances and need to be corrected with long dipole coils along the undulator or sufficiently attenuated by shielding.

During the BBA procedure, the undulator segments will be at the fixed Tuning Gap as measured with linear encoders, which have been calibrated during the tuning process in the magnet measurement lab. It is expected that undulator field integrals will significantly vary as the gap is changed. This will change electron beam steering, which will be corrected with the dipole correctors that are incorporated into the quadrupole magnets.

The required corrections will first be measured in the magnet measurement lab and later fine-tuned based on RFBPM readings. This is similar to what is currently done at LCLS, where field integrals change and quadrupoles move (due to girder twist) as undulator segments are moved in and out.

During initial installation of the components, the quadrupole magnets will be aligned to a straight line within a local error of 100 μm (rms) and a walk-off amplitude of less than 250 μm . Both, the quadrupoles and the undulator jaws will be equipped with tooling balls that will have been fiducialized to the magnetic axis of the devices. For the undulator this fiducialization will be done at the Tuning Gap.

The undulators, which will be installed independently of the quadrupole magnets, will then be aligned in the tunnel such that their magnetic axes are centered between the magnetic axes of



the neighboring quadrupoles. This procedure has been successfully applied several times for the LCLS undulator segments since operations began. Using laser trackers, a precision of about 50 μm (rms) can be achieved. This alignment technique will be repeated after the first beam based alignment procedures have been applied setting the quadrupoles to the correct positions to allow FEL operation. Encoders that would allow measurements of the relative position between the quadrupole center and the undulator strongback would aid this process and their availability is desirable.

The vacuum chamber, which needs to be centered on the electron beam, will be supported off the adjacent quadrupole support movers and aligned relative to the quadrupole centers during the initial alignment procedure. It is expected that the initial BBA procedure will move the quadrupole positions by less than 500 μm . The vacuum chamber will move with the quadrupoles. The position of the undulator segment strongbacks will need to be adjusted to stay centered on the vacuum chamber. There will be sufficient clearance between the quadrupole magnets and the vacuum chamber to allow for this movement. Once lasing has been achieved, BBA will move the quadrupole magnets by less than $\pm 60 \mu\text{m}$, based on LCLS experience. In LCLS, there are indication that the BBA procedure does not put the electron beam onto a straight line over the entire undulator line but can leave long-range bows in the trajectory with sagitta amplitudes in the order of 20 μm , which can cause the x-ray beam to change at the experimental stations after BBA procedures as well as when changing the number of active undulators. This is currently under investigation at LCLS. It is expected that the additions of extra constraints in the BBA algorithm will reduce the problem, significantly.

9 End Notes

- i. Z. Huang, K.J. Kim(2007). "Review of x-ray free-electron laser theory". *Physical Review Special Topics - Accelerators and Beams* 10 (3). doi:10.1103/PhysRevSTAB.10.034801
- ii. *Linac Coherent Light Source (LCLS) Conceptual Design Report*, SLAC-R-593, U-414 (2002) – Chapter 8
- iii. Li, Y., Faatz, B. & Pflueger, J. *Undulator system tolerance analysis for the European X-ray free-electron laser*. *Phys. Rev. Spec. Top. AB* 11, 100701 (2008)
- iv. LCLS-II "Undulator Phase Shifter" PRD, LCLSII-3.2-PR-0105.
- v. Z. Wolf, Y. Levashov, *Beam Pipe Corrector Study*. LCLS-TN-12-1 (March 2012)
- vi. J.C. Dooling, W. Berg, B.X. Yang, M.S. Leitner, A.S. Fisher, H.-D. Nuhn, *Modeling the Optical Coupling Efficiency of the Linac Coherent Light Source Beam Loss Monitor Radiator*, BIW 2010, JACOW (2010).
- vii. H.-D. Nuhn, G. Gassner, F. Peters, "Position Stability Monitoring of the LCLS Undulator Quadrupoles," SLAC-PUB-14891.
- viii. K.L.F. Bane, G.V. Stupakov, *Resistive Wall Wakefield in the LCLS Undulator*, Proceedings of the 2005 Particle Accelerator Conference, PAC2005.
- ix. H.-D. Nuhn, P.J. Emma, G.L. Gassner, C.M. LeCocq, F. Peters and R.E. Ruland, *Electron Beam Alignment Strategy in the LCLS Undulators*, FEL2006 Proceeding, 2006, Berlin, Germany.